# MOLECULAR AND MICROSCALE HEAT TRANSFER

Edited by
**Susumu Kotake** and **Chang-Lin Tien**

under the Auspices of
**Thermal Science and Engineering,**
**The Heat Transfer Society of Japan**

**Begell House, Inc.**
New York • Wallingford (U.K.)

**Molecular and Microscale Heat Transfer**



**Library of Congress Cataloging-in-Publication Data**

Molecular and microscale heat transfer / edited by Susumu Kotake and Chang-Lin Tien ; under the auspices of Thermal Science and Engineering, The Heat Transfer Society of Japan.
p. cm.
Includes bibliographical references.
ISBN 1-56700-017-7
1. Heat--Transmission. I. Kotake, Susumu, 1934- . II. Tien, Chang L., 1935- . III. Nihon Dennetsu Gakkai.
TJ260.M565 1994
621.402'2--dc20 94-10525
CIP

# Preface

Molecular and microscale thermal science and engineering is an emerging field in the heat transfer community. The last few years have witnessed a steady increase in the number of papers published and in the number of conference sessions organized on this topic. The excitement in this field of microscale or nanoscale phenomena is not only in thermal sciences but in science and engineering in general. Therefore it was felt that it is timely to organize a special forum on this topic. Due to the rapidly increasing activity in this area in both Japan and the USA, a joint seminar was planned with the following goals:

(i) to assess the accomplishments and to determine the future needs;
(ii) to address some of the open scientific and engineering questions;
(iii) to increase the awareness of the researchers with regards to the industrial demands and to the research conducted in other disciplines;
(iv) to provide a forum to present new results; and
(v) to increase interdisciplinary and international collaboration.

The seminar, held in Kanazawa, Japan on July 11-14, 1993, was supported by the Japan Society for the Promotion of Science (JSPS) from the Japanese side and by the National Science Foundation (NSF) from the US side. This book contains the papers that were presented at this seminar. A report contains the papers that were presented at this seminar. A report containing a critical assessment of the seminar will also be published soon in the Annual Review of Heat Transfer (Volume 7). Hopefully, these papers and the critical report will raise some important issues and questions that need to be addressed in the future.

We wish to express our deep gratitude to Professors Kunio Hijikata, Markus Flik and Arun Majumdar for their outstanding contributions to the forum preparation and their editorial assistance to this book.

Chang-Lin Tien (Berkeley, USA)
Susumu Kotake (Tokyo, Japan)

## CONTENTS

# Microscale Thermal Phenomena In Contemporary Technology *

Cheng Lin TIEN†, Tai Qing QIU† and P.M. NORRIS†

## Abstract

Great progress has been made in recent years in fabricating micro-devices and materials with novel microstructures, such as microelectronic devices, microelectromechanical systems, and advanced materials. In the area of thermal science this development has caused a shift in thermal phenomena from macroscale to microscale, which presents not only new challenges but also new opportunities to achieve a better understanding and control of energy transfer. This paper addresses microscale thermal phenomena in three general areas: micro-length scale phenomena, microstructures, and micro-time scale phenomena.

KEYWORDS: *Microscale heat transfer*

## Nomenclature

| | | |
|---|---|---|
| a | = | lattice constant, m |
| c | = | speed of light, m/s |
| C | = | heat capacity, $J/m^3K$ |
| $d$ | = | radiation penetration depth, m |
| $d_f$ | = | fractal dimension |
| $e_b$ | = | total blackbody emissive power, $W/m^2$ |
| $e_{b,\lambda}$ | = | spectral blackbody emissive power, $W/m^3$ |
| E(T) | = | extinction coefficient, $m^{-1}$ |
| $E(\lambda)$ | = | spectral extinction coefficient, $m^{-1}$ |
| G | = | electron-lattice coupling factor, $W/m^3K$ |
| $\hbar$ | = | Planck's constant divided by $2\pi$, Js |
| k | = | thermal conductivity, W/mK |
| $k_{g,o}$ | = | thermal conductivity of free gas, W/mK |
| Kn | = | Knudsen number |
| L | = | characteristic length, m |
| $l$ | = | temperature penetration depth, m |
| l | = | coherence length, m |
| $l_g$ | = | mean free path, m |
| m | = | mass, kg |
| $m_e$ | = | electron mass, kg |
| n | = | electron number density, $m^{-3}$ |
| $\bar{n}$ | = | number density, $m^{-3}$ |
| Q | = | heat flux, $W/m^2$ |
| S | = | heating source, $W/m^3$ |
| t | = | time, s |
| $t_h$ | = | characteristic heating time, s |
| $t_c$ | = | electron-lattice thermalization time, s |
| T | = | temperature, K |
| v | = | velocity, m/s |
| V | = | volume, $m^3$ |
| x | = | distance, m |
| $\Phi$ | = | effective pore diameter, m |
| $\kappa$ | = | Boltzmann's constant, J/K |
| $\lambda$ | = | photon wavelength, m |
| $\Lambda$ | = | heat carrier mean-free-path, m |
| $\theta_D$ | = | Debye temperature, K |
| $\rho$ | = | density, $kg/m^3$ |
| $\sigma$ | = | Stefan-Boltzmann constant, $W/m^2K^4$ |
| $\tau$ | = | relaxation time, s |
| $\xi$ | = | characteristic length, m |

### Subscripts

| | | |
|---|---|---|
| c | = | heat carrier |
| e | = | electron |
| g | = | gas |
| l | = | lattice |
| r | = | radiative |
| s | = | solid |

## 1 Introduction

Modern technology has seen tremendous progress in fabricating microelectronic and optoelectronic devices with higher operation speeds, larger memory, and higher output powers by synthesizing more sophisticated materials and developing more efficient and advanced processing techniques. Accompanied with these trends is a shift of dominating thermal phenomena from macroscale to microscale. Examples include the thermal control of electronic circuits and quantum well lasers [1], thermal design of micro cooling devices [2], structural design of advanced thermal insulating materials [3], quality control of short-pulse laser processing [4], and short-pulse laser diagnostics [5]. These abundant microscale thermal phenomena present not only new challenges but also new opportunities for thermal engineers to achieve a better understanding and control of energy transfer.

Microscale heat transfer becomes important when the feature length of a device is comparable to or smaller than the heat carrier mean-free-path. Consequently, thermal properties of materials become dependent on structure and heat conduction processes are no longer local phenomena, but are nonlocal, radiative phenomena. The restriction of heat carriers by device geometry can significantly reduce the thermal conductivity [6]. This effect is not desirable in electronic packaging, but it is a desirable effect for thermal insulation. The nonlocal feature of heat conduction in small structures requires microscopic energy-transfer models rather than the conventional macroscopic Fourier conduction model [7]. It is necessary to classify energy transfer regimes at different length scales and to describe principles governing the

* Received: Oct. 15 1993

† Department of Mechanical Engineering University of California Berkeley, CA 94720, USA

Modern microfabrication technology provides great opportunities to actively process materials at micro- and nanometer scales, and thus generates devices with novel thermal properties. Examples include the dramatic modification of surface radiation properties by micromachining [8], the high frequency response of heat flux microsensors [9], and the ultra-low thermal conductivity of silica aerogels [10]. New theories are needed to characterize microstructures and their interactions with energy transfer.

The advent of short-pulse and high-power lasers has made it possible to observe novel phenomena and to control extraordinary processes at a new energy level and on new spatial/temporal scales. Laser intensities have reached $10^{19}$ W/cm$^2$ so far and they are projected to reach $10^{24}$ W/cm$^2$, which is more than twenty orders of magnitude larger than the radiation intensity at the surface of the sun, in the near future [11]. The laser pulse duration has also decreased dramatically in the last three decades, reaching the fundamental limits set by the properties of light [12]. For example, modern techniques have created optical pulses that are only six femtoseconds in duration [13]. Due to the high energy transfer rate and the short interaction time, applications of high-power and short-pulse lasers require a microscale understanding of energy transfer processes.

This work addresses microscale thermal phenomena in three general areas, with a focus on solid materials: (1) micro-length scale phenomena, (2) microstructures, and (3) micro-time scale phenomena. Emphasis is placed on characterization of thermal properties and energy transfer in the microscale domains and potential applications of microscale thermal phenomena to advanced technology.

## 2 Exp riment

Micro-length scale heat transfer has emerged as an active research area in thermal science due to the increasing desire to understand thermal phenomena in thin films and microstructures [14, 15]. Thin films used in modern electronic, optical, and optoelectronic devices span several orders of magnitude in thickness — from a few nanometers to several hundred microns. An accurate description of the physical processes in thin films generally requires the use of more fundamental physical laws and equations than those used for bulk media. For example, the design of an interference filter must be based on Maxwell's electromagnetic wave equations rather than on geometrical optics, while the latter can be used to design lenses [16]. In electronics, carrier transport in submicron devices is more often modeled by the Boltzmann transport equation (BTE) or the Monte-Carlo method rather than by employing the carrier diffusion equation [17]. In quantum well lasers, where the film thickness is less than 20 nm, quantum mechanics must be applied [18]. These examples demonstrate why the validity of macroscopic heat transport theories must be questioned when investigating micro-length scale phenomena.

Traditional heat transfer, or macroscale heat transfer, employs phenomenological laws, such as Fourier's law, without considering the detailed motion of the heat carriers. Microscale heat transfer involves heat transfer processes when the heat carrier (electrons, phonons, and photons) mean-free-path (MFP) is on the same order of magnitude or even larger than the characteristic device dimension, such as the film thickness [19]. Much research has been devoted to microscale heat transfer phenomena in cryogenic systems because the heat carrier MFP is larger at low temperatures. Examples include cryogenic multilayer-insulation systems, spacecraft thermal control coatings, and superconducting thin films. Modern microfabrication technology is reducing device dimensions into the micro- and nanometer scales, however, thus making microscale heat transfer processes important even at room temperature.

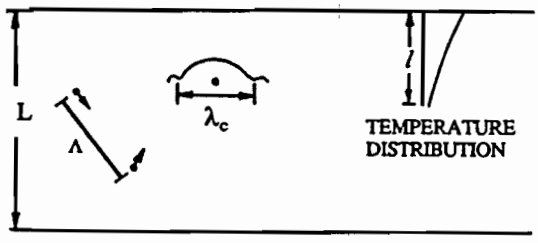


**Figure 1** Characteristic lengths in conduction

### 2.1 Characteristic Lengths in Heat Conduction

Heat is conducted in solids through free electrons and phonons. In metals, free electrons dominate the heat conduction, while in insulators and semiconductors, phonons are the major heat carriers. An examination of the various characteristic lengths of heat carriers leads to the definition of two microscale heat conduction regimes.

The characteristic lengths for heat conduction are the heat carrier MFP, $\Lambda$; the characteristic device dimension, L; the temperature penetration depth, $l$; and the heat carrier wavelength, $\lambda_c$. These characteristic lengths are illustrated in Fig. 1. The heat carrier MFP, $\Lambda$, is the average distance that a carrier travels in a bulk material before its excess energy is lost. It is determined by the various scattering mechanisms in the solid, including scattering by phonons, electrons, impurities, and imperfections. These mechanisms, and thereby the heat carrier MFP, are strongly dependent on temperature.

The temperature penetration depth, $l$, characterizes the temperature gradient and is here defined as a characteristic temperature divided by the maximum temperature gradient,

$$l = T / (dT/dx)_{max} \quad (1)$$

This is not an intrinsic property of the heat carrier but may depend on time, heat source distribution, and the thermophysical properties of the material. This characteristic length becomes important in fast heating processes.

Due to the wave-particle duality, both electrons and phonons have a characteristic wavelength, $\lambda_c$. The characteristic electron wavelength is its thermal de Broglie wavelength [20],

$$\lambda_c = \hbar / \sqrt{2\pi m_e \kappa T} \quad (2)$$

where $\hbar$ is Planck's constant divided by $2\pi$, me is the effective electron mass, and $\kappa$ is Boltzmann's constant. At high temperatures (above the Debye temperature, $\theta_D$), the dominant

phonon wavelength is on the order of the lattice constant, a. At low temperatures, the characteristic phonon wavelength is on the order of $\theta_D a/T$ [21].

When the characteristic device dimension is larger than the heat carrier MFP, heat conduction is in the macroscopic regime and is thus governed by Fourier's law. Conversely, when the MFP is larger than the characteristic dimension, then heat conduction is in the microscopic region and depending on the relative magnitude of the various characteristic lengths described above, two microscale heat conduction regimes can be identified.

The first microscale heat conduction regime is characterized by classical size effects and nonlocal energy transport. This regime is defined when

$$i)\ L/\Lambda < O(1) \quad \text{or} \quad l/\Lambda < O(1) \tag{3a,b}$$

and

$$ii)\ L/\lambda_C > O(1) \tag{4}$$

Notice that only an order of magnitude sign is used for all these definitions. Flik et al. [22] showed that the size effects on heat conduction become important when $L<7\Lambda$. Additional research efforts should be directed towards quantitative demarcation of the heat conduction regimes. When Eq. (3a) holds, the heat carrier MFP is limited by the boundary scattering in addition to the internal scattering mechanisms. When Eq. (3b) is true, heat carriers experience a large temperature difference within one MFP. For both cases, the Boltzmann transport equation can be used to describe the distribution function of heat carriers [23].

Solution of the BTE yields the heat flux, which in combination with the first law of thermodynamics gives the equation governing the temperature distribution [7, 24]. In the first microscale regime thermal conductivity is no longer an intrinsic property but depends on heating conditions and the size, shape, and boundary of the devices. Therefore the question arises whether the thermal conductivity or some other more fundamental parameters such as the relaxation time or scattering rate should be used to describe heat conduction.

The second microscale regime is defined when the characteristic heat carrier wavelength of the material is on the same order or larger than the characteristic dimension,

$$L/\lambda_C < O(1) \tag{5}$$

In this regime, quantum size effects become important. The BTE has been used to describe the electron transport properties in quantum structures [25]. Applicability of the BTE to the second microscale heat transfer regime has not been examined. Wakuri and Kotake [26] used the molecular dynamic equation based on the argument that the BTE is a statistical equation, and the use of statistics is no longer valid when the film is very thin. Work should be done to compare the results obtained from the Boltzmann transport equation and from the molecular dynamics approach.

## 2.2 Characteristic Lengths in Thermal Radiation

Figure 2 illustrates the characteristic lengths for radiation. In addition to the characteristic lengths required for heat conduction, the photon wavelength, $\lambda$, and photon coherence length, $l_C$, are important in thermal radiation [16]. The characteristic radiation wavelength depends on the radiation source. For a thermal source, it is given by Wien's displacement law as,

$$\lambda T = 2989\ \mu m\ K \tag{6}$$

The photon coherence length is the maximum optical path difference between two wave trains from the same light source before their interference ability is lost. Metha [27] gave the coherence length of blackbody radiation in a vacuum as

$$l_C = 0.3\pi c\hbar/\kappa T \tag{7}$$

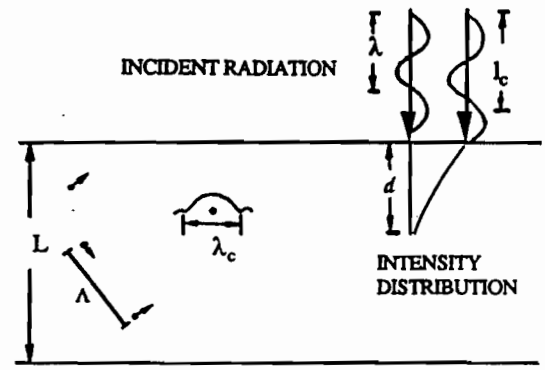


**Figure 2** Characteristic lengths in radiation

The radiation penetration depth, $d$, characterizes the absorption in the medium and is defined as the depth at which the intensity is attenuated to 1/e of its value at the surface.

Three microscale radiation heat transfer regimes may be defined based on the relative magnitude of the various characteristic lengths. The first microscale radiation regime is defined when

$$L/l_C < O(1) \tag{8}$$

Again only an order of magnitude is used, as exact demarcation of the first microscale radiation regime depends on the application. In this regime, the optical constants of the material are not affected by the size and boundary of the device, however, the derived radiative properties, such as the reflectance, transmittance, and scattering cross-section must include the wave nature of the radiation and are obtained through the solution of Maxwell's electromagnetic wave equation [16].

Some specific criteria have been established to delineate the first microscale and the macroscale radiation regimes. Tien [28] summarized radiation in particulate systems and presented regime maps for dependent and independent scattering. Tuntomo et al. [29] considered internal absorption for a single particle and compared the wave optics and intensity superposition results. Chen and Tien [30] and Richter et al. [31] constructed regime maps to delineate the first microscale and macroscale radiation regime for thin films based on the coherence theory of light.

Radiative transfer in the first microscale regime can be described in two ways. If the thermal emission from the media is not important, the solution of Maxwell's EM wave equation will

give the radiation intensity distribution inside the medium. When thermal emission is important, the equation of radiative transfer should be used [32], but with the radiative properties appropriate for the first microscale regime.

The second microscale radiation regime is characterized by classical size effects on the fundamental optical properties and is defined when

$$i)\quad L/\Lambda < O(1) \quad \text{or} \quad d/\Lambda < O(1) \tag{9a,b}$$

and

$$ii)\quad L/\lambda_c > O(1) \tag{10}$$

When Eq. (9a) holds, the boundaries impose a limit on the carrier momentum MFP and classical models such as the Drude and Lorentz models can be used for the optical constants, but with a modified $\Lambda$. Similar to heat conduction, the boundary and interface conditions affect $\Lambda$ in this regime and thus the optical constants [33]. If Eq. (9b) holds, then electrons traveling one $\Lambda$ experience a non uniform electromagnetic field. This nonlocal transport of electrons is called the anomalous skin effect [34].

The third microscale regime is defined when

$$L/\lambda_c < O(1) \tag{11}$$

In this regime quantum size effects become important. These include the change of electronic band structures and phonon spectra, and the discretization of the available quantum states. An example is the quantization of optical properties in a quantum well [18]. The optical constants can be calculated from principles of quantum mechanics and solid state physics.

Based on the characteristic lengths of the heat carriers, two microscale heat conduction and three microscale radiation regimes are defined. The first and second heat conduction microscale regimes are characterized by the classical and quantum size effect on heat conduction, respectively. In the first microscale radiation regime, the wave nature of the radiation field must be considered. In the second and third microscale radiation regimes, the classical and quantum size effects modify the optical properties of thin films, respectively. The challenge remains to clearly delineate the microscale heat transfer regimes and to obtain the thermal radiative properties and radiant heat source distributions in microstructures.

## 3 Microstructures

The advance of modern microfabrication technology has generated great excitement, opening up new areas of research to meet challenges in the fabrication of more advanced devices, development of more sophisticated sensors, and the processing of materials with novel properties. Microfabricated thermal devices provide more precise and enhanced control of heat generation, heat flow, mass flow, and phase change. Examples include micro-metal-wire heaters, micro-heat pipes, microchannels, microlamps, microvalves, micropumps, micro jet nozzles, and microevaporators [14]. Such devices have been used in ink-jet printers, in cooling systems for high-power diode lasers, and for microscale control of cell growth in artificial organ applications; and their areas of application are only expected to grow. For example, the steam power generated in microevaporators could be used in actuator applications, since it can deliver larger forces than commonly employed electrostatic and piezoelectric forces. Microsensors are not merely miniaturized versions of conventional sensors, they have unique features and thus provide opportunities to study new phenomena with high spatial and temporal resolution, such as energy transport in thin films and micro-devices.

The microstructure of a material determines its thermal properties. Thus, by designing and processing materials with appropriate microstructures, one can produce materials with desired properties. One of the most successful examples is the development of aerogel, a foam material with ultra fine pore sizes and ultra low solid-volume fraction. Due to their high porosity and large inner surface area, aerogels offer much potential as catalysts, thermal insulators, adsorbents, fillers, building materials, pigments, reinforcement agents, and acoustic insulators. This section focuses on a better understanding of the interaction of aerogel microstructures and energy transfer.

### 3.1 Aerogels - Production Methods

The manufacture of gels is generally referred to as the sol-gel process. Starting from a chemical solution that contains inorganic salts or metal organic compounds, clusters or polymeric chains grow and form a coherent gel network that is embedded in a liquid phase [35, 36]. In order to obtain an aerogel, the liquid phase of the gel must be removed and replaced by a gas. However, drying of the gel by evaporation under ambient conditions leads to considerable shrinkage of the gel network due to capillary forces that partially collapse the fragile solid structure [36]. In 1931 Kistler succeeded in drying gels without collapsing their solid skeletons by supercritically expanding the fluid filling, thereby avoiding the formation of liquid-vapor interfaces. This resulted in a gas-filled, intact gel structure [37].

The structure generated by the sol-gel process can be described by the concepts of fractal geometry on some length scales. The initial phase of gelation, i.e., the growth of complexly branched clusters in a liquid phase, is described by the theory of colloidal aggregation [38]. Experimental observations [39] as well as theoretical predictions show that the mass, m, of a forming cluster is related to a characteristic length, $\xi$, by the scaling relationship

$$m \propto \xi^{d_f} \tag{12}$$

where the exponent $d_f$ is the mass fractal dimension of the structure. For instance, the cluster shown in Fig. 3 has the dimension $d_f = 1.71$ [38], describing the fact that the conglomerate gets continuously sparser as the cluster grows. This phenomenon occurs because the outer branches of the cluster shield the inner voids of the structure. For purely statistical reasons, particles that approach the cluster by diffusion have a strong tendency to be deposited on the most outward branches. This leads to a cluster volume that grows faster than its mass which is reflected by a fractal dimension smaller than the Euclidean dimension of the object.

Silica aerogels are composed of small silica particles (diameter ~ 5 nm) aggregated into fractal clusters or micro-gels which collide to form a homogeneous gel. From a macroscopic point of view, the gel appears to be homogeneous, typically

having a solid volume fraction between 0.1 and 10 percent. If the structure is investigated with a resolution on the order of the cluster diameter (5 to 200 nm), a fractal mass distribution can be observed. For even smaller length scales, the material characteristics are dominated by the silica particles. The microstructure of a silica aerogel is shown in Fig. 4 [40].

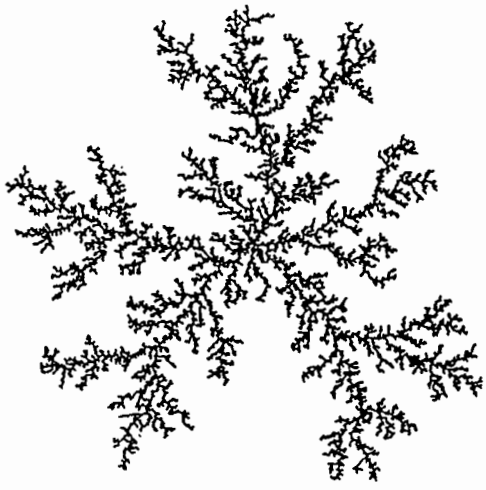

**Figure 3** Cluster with fractal dimension $d_f$=1.71 [38]

## 3.2 Novel Applications - Insulation and Catalysis

The unique structure of silica aerogels leads to very unusual material properties. Two areas that offer great potential for saving primary energy resources are thermal insulation and catalysis. Kistler [41] showed that aerogels have an extremely low thermal conductivity, ranging from 0.02 W/mK under ambient conditions to 0.01 W/mK for evacuated samples. Additionally, as opposed to all other common insulators, silica aerogels can be made transparent in the visible range of the electromagnetic spectrum, making it possible to use them in window insulations [42, 43] and passive solar energy devices [44-46].

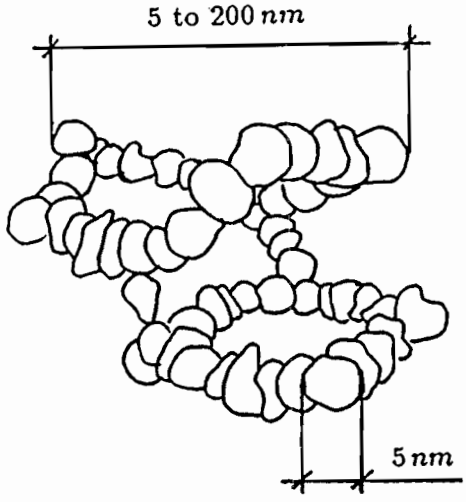


**Figure 4** Aerogel microstructure [40]

Generally speaking, a catalyst is a substance that accelerates the rate at which a chemical reaction approaches equilibrium while the catalyst itself remains basically unchanged. Since catalytic reactions take place at the surface of the catalyst, it is advantageous to use a substance with a large surface area accessible to the reactions. Aerogels have extremely high surface areas and pore volumes and therefore have a great potential for application in catalysis. Another advantage of aerogel-based catalysts is their excellent textural stability at high temperatures. Amorphous silica and alumina gels, for instance, have a surface area of several hundred square meters per gram even after a 600°C heat treatment [47]. For most conventionally prepared catalysts, however, sintering or other structural changes occur around this temperature, leading to a substantial decrease in active surface area and a fast deterioration of catalytic power.

## 3.3 Heat Transfer Phenomena

Three different mechanisms contribute to the heat transfer in aerogels: radiation, gaseous conduction via the pore-filling gas, and solid conduction through the gel network. Although these three contributions are generally interdependent and can only be analyzed by numerically solving a complex integro-differential equation [32], they can approximately be linearly superimposed if the assumption of an optically thick medium holds. The total conductivity, $k$, of an aerogel can be written as

$$k = k_r + k_g + k_s \tag{13}$$

where $k_r$ represents an effective radiative conductivity, $k_g$ is the conductivity of the gas filling, and $k_s$ is the conductivity of the solid network [3].

For optically thick media radiation can be treated as a diffusion process, and the radiative conductivity $k_r$ can be calculated from the known extinction properties of the medium [32],

$$k_r(T) = \frac{16}{3} \cdot \frac{n^2 \sigma T^3}{\overline{E}(T)} \tag{14}$$

with the refractive index n and the Stefan-Boltzmann constant $\sigma$. The averaged extinction coefficient, $\overline{E}(T)$, is evaluated by integrating over all wavelengths and employing the Rosseland weight function,

$$\frac{1}{\overline{E}(T)} = \int_0^\infty \frac{1}{E(\lambda)} \cdot \frac{\partial e_{\lambda,b}(T)}{\partial e_b(T)} d\lambda \tag{15}$$

where $e_b$ is the total blackbody emissive power and $e_{\lambda,b}$ is the spectral blackbody emissive power of a surface at temperature T. The spectral extinction $E(\lambda)$ can be derived from transmissivity measurements.

In the case of thin aerogel layers, however, one can no longer assume an optically thick medium. The direct exchange of radiative energy between the interfaces may be significant, depending on temperature, and a modified diffusion model with proper boundary conditions is required. A radiative pseudo-conductivity $k_r$, that degenerates into the expression for optically thick media and depends on the thickness of the aerogel layer can be defined for optically thin aerogels.

Though aerogels can be made transparent to visible light,

there is appreciable infrared extinction caused by absorption. Aerogels are opaque to infrared radiation above wavelengths of 7 μm, however, a large transmission window exists for wavelengths between 3 and 7 μm. Therefore, at low temperatures (T < 300 K) radiative transport is weak. For increasing temperatures, however, more and more radiation can penetrate the aerogel [20]. If the aerogel does not have to be transparent the transmission window in the infrared can be considerably reduced by opacifying the gel. Such gels are high performance, non-toxic, and non-combustible substitutes for conventional polyurethane foam insulations.

In gases heat is conducted via the motions and collisions of the gas molecules, as described by statistical mechanics. The thermal conductivity $k_g$ of a gas can be written as

$$k_g = \bar{n} \cdot \kappa \cdot l_g \cdot v \tag{16}$$

where $\bar{n}$=N/V is the number density of the gas molecules, κ is Boltzmann's constant, $l_g$ is the mean free path, and v is the average velocity [10]. For air at ambient conditions, the mean free path, $l_g$, is about 70 nm. Aerogels have pores that lie in the same size region, and according to Knudsen's equation, the conductivity of a gas that fills such a structure varies with the effective pore diameter Φ as

$$k_g = \frac{k_{g,o}}{1 + \beta Kn(\Phi)} \tag{17}$$

The parameter $\beta \approx 2$ for air and $k_{g,o}$ is the conductivity of the free gas. The Knudsen number Kn is defined by

$$Kn = l_g / \Phi \tag{18}$$

and is on the order of one for aerogels at ambient conditions. Consequently, the gaseous conductivity in aerogels is considerably lower than that for free gas at ambient conditions. Kistler [41] showed that for low pressures (less than 100 mbar), gaseous conductivity of aerogels is negligible because the Knudsen number is large, but for higher pressures, the mean free path $l_g$ decreases and becomes comparable to the effective pore diameter Φ, resulting in a steep increase in the gaseous conductivity. In Kistler's experiment [41] the total conductivity $k$ increased from 0.012 W/mK for an evacuated aerogel sample to 0.02 W/mK at ambient pressures.

Heat transfer via the solid skeleton has only very recently been studied in much detail [40]. The solid conductivity of silica aerogels is much smaller than that of vitreous silica due to the gel's extremely ramified microstructure which impedes heat diffusion by increasing the path lengths for the conductive process. Massive silica glass has a thermal conductivity of 1.4 W/mK compared to a silica aerogel sample with a density of ρ = 71 kg/m$^3$, for instance, which has a solid conductivity ranging from about $3 \times 10^{-6}$ W/mK at extremely low temperatures (T < 1 K) to about $2 \times 10^{-3}$ W/mK at ambient temperatures [40].

Solid conduction is closely related to the structural properties of aerogels. At temperatures below 1 K, heat transfer is governed by low frequency phonons whose wavelengths are above the pore size of the gel microstructure. In this region, the gel structure appears to be homogeneous and the propagation speed of phonons is equal to the velocity of sound in the gel (v ~ 100 m/s). At higher temperatures, oscillations of much higher frequency and shorter wavelength are excited, including vibrational modes of the individual gel particles. For these phonons the mean free paths are greatly reduced. This tremendous increase of vibrational modes for temperatures above 50 K leads not only to a much higher conductivity, $k_s$, but also to an increase in the gel's heat capacity [40].

If the surface temperature of an aerogel were measured as a function of time, and hence diffusion length, it would have the same general shape as the curve shown in Fig. 5 [48], which is the time-dependent surface temperature of an assembly of slightly bonded spheres. The temporal dependence exhibits three distinct slopes, corresponding to the three length scales in aerogels. Below a few hundred microseconds, diffusion occurs within the first layer of irradiated spheres and the diffusion is Euclidean, hence the slope is one-half. This corresponds to diffusion on the length scale of the individual silica particles. Then the heat begins to diffuse between spheres through a random network of bonds and the slope decreases to 0.2. This corresponds to the fractal regime in aerogels, which occurs on length scales between the diameter of the silica particles and the cluster diameter. Finally, for times longer than 0.15 s the diffusion is Euclidean again with a slope of one-half since the heat has covered a distance larger than the biggest hole in the network structure. This corresponds to a length scale larger than the cluster diameter. The existence of these three scales greatly complicates the evaluation of heat transfer in aerogels but may lead to some novel applications.

Aerogels are fascinating materials with potential for wide application in varied fields. As advances are made in processing the ultra fine structure of aerogels, better control of the macroscopic properties of the material will be gained. By altering the microstructure, aerogels can be designed to optimize their use in specific applications. However, while many efforts have been made to model the structure of aerogels, much work remains to better understand the interrelationship between aerogel structures and heat transfer phenomena on the micro-scale.

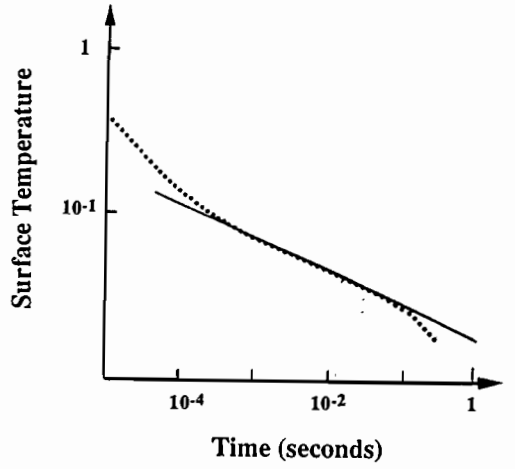


**Figure 5** Transient surface temperature of slightly bonded spheres [48]

## 4 Micro-Time Scale Phenomena

Lasers have altered both the course and pace of the development of science and technology since their invention

thirty years ago. Laser applications have fundamentally shaped modern technology in the areas of measurement, materials, manufacturing, information, and communication.

Figure 6 shows energy regimes of typical laser applications. For continuous lasers, the interaction time represents the time needed for the laser spot to scan one diameter relative to the material surface, and for pulse lasers, it represents the laser pulse duration. This characteristic time can range from the continuous interaction regime down to the molecular time-scale regime ($10^{-14}$ s). Laser intensities in these applications range from the equivalent radiation intensity at the surface of the sun to a level that is twelve orders of magnitude larger.

Modern lasers have also greatly increased the time resolution of optical observations and the spatial controllability of optical processing. Since the invention of lasers the achievable optical pulse duration has been reduced dramatically from microseconds to femtoseconds, reaching the fundamental limits set by the properties of light [12]. Such short femtosecond laser pulses are more than adequate to perform detailed stop-action optical observations of a wide variety of previously inaccessible phenomena. In addition, short-pulse lasers provide superior spatial controllability for optical diagnostics and processing.

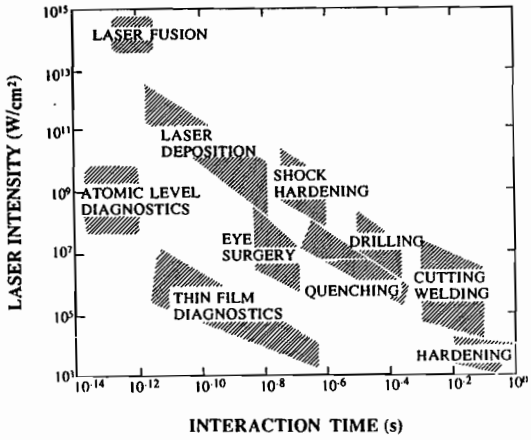


**Figure 6** Energy regimes of laser applications

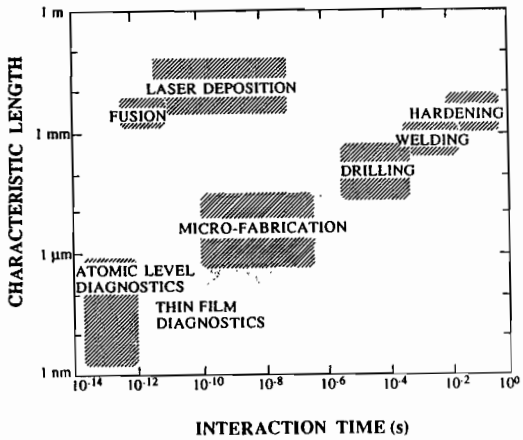


**Figure 7** Size regimes of laser applications

The minimum size of the laser affected region in materials is the radiation absorption volume, which is determined by the laser-beam cross-section and the radiation penetration depth. The actual size, however, is always larger than the radiation absorption region due to thermal diffusion. Reducing laser-material interaction time reduces the degree of thermal diffusion, which in turn localizes laser energy.

Based on this principle, short-pulse lasers are now used for the diagnosis and fabrication of microstructures, such as measuring thin-film properties [5], drilling tiny holes in jet engine blades for cooling [49], and repairing micro-electronic devices [50, 51].

Energy transport plays a significant role in the application of high-power and short-pulse lasers. Due to the extremely high heat flux and short interaction times encountered in laser applications, applicability of conventional thermal models is subject to question. A more accurate microscale understanding of energy transfer is necessary.Figure 7 shows length regimes of typical laser applications. The characteristic length represents the most interesting length scale in the application, for example, the hole diameter in laser drilling, diameter of fuel pellets in laser fusion, feature length in micro-fabrications, and spatial resolution in laser diagnostics.

### 4.1 Microscopic Energy Deposition and Transport

Two very fundamental issues in the study of energy transport are how to define appropriate parameters to describe thermodynamic states of a material and how to use these parameters to characterize energy flux in the material. Conventionally, a single temperature of the material is used to describe its thermodynamic state and the Fourier conduction model can be used to characterize energy flux by heat conduction. In the application of high-power and short-pulse lasers, however, more profound theories are needed to handle thermal problems in such a novel energy-flux and time-scale regime. The theories should be able to answer three fundamental questions: (1) how energy deposits itself in materials under an extremely strong radiation flux, (2) how energy propagates in an extremely short period of time, and (3) how materials behave in the high energy-flux and short time-scale regime.

Laser-material interactions involve complicated energy transport processes among microscopic energy carriers. There exist two kinds of energy carriers in metals: free electrons and vibrations of the metal lattice. During low-power and long-pulse laser heating, the microscopic electron-lattice interactions are quick enough to restore thermal equilibrium between electrons and the lattice. As a result, the dynamics of the microscopic processes are not important and the macroscopic approach is applicable. On the other hand, during high-power and short-pulse laser heating, the time scale of the microscopic electron-lattice interactions becomes comparable to the characteristic laser heating time; consequently, detailed dynamic information of microscopic processes becomes very important.

Qiu and Tien [24] derived a hyperbolic two-step radiation heating model (HTS) for metals from the Boltzmann transport equation of electrons as

$$C_e(T_e)\frac{\partial T_e}{\partial t} = -\nabla \cdot Q - G(T_e - T_l) + S \tag{19}$$

$$C_l(T_l)\frac{\partial T_l}{\partial t} = G(T_e - T_l) \tag{20}$$

$$t\frac{\partial Q}{\partial t}+\frac{T_e}{T_l}k\nabla(T_e)+Q=0 \tag{21}$$

where $T_e$ and $T_l$ are the electron and the lattice temperature, respectively, $C_e$ and $C_l$ are the electron heat capacity and the lattice heat capacity, respectively, G is the electron-lattice coupling factor, $\tau$ is the electron relaxation time, and k is the thermal conductivity. This model describes radiation deposition in metals as a two-step process: heating of free electrons and the subsequent energy redistribution between electrons and the metal lattice. Equation (19) describes the change of the electron energy as the result of heat transport by electrons, energy exchange between electrons and the lattice, and radiation absorption. Equation (20) describes heating of the lattice through electron-lattice coupling. Heat diffusion by the lattice in Eq. (20) is neglected since free electrons are the dominant energy carriers in pure metals. Equation (21) shows that in the micro-time scale heat flux depends not only on the electron temperature gradient but also on the history of the heat flux itself.

The HTS model can lead to existing models depending on the relative magnitude of three characteristic times during laser heating: (1) the characteristic heating time, $t_h$, which represents either the laser pulse duration or the time needed to heat a material to a certain temperature, (2) the electron relaxation time, $\tau$, and (3) the electron-lattice thermalization time, $t_c=C_e/G$, which is the time needed for electrons and the lattice to reach thermal equilibrium. When the characteristic heating time is much greater than the relaxation time, the effect of hyperbolic energy transport is small; consequently, the HTS model becomes the parabolic two-step model (PTS) of Anisimov et al. [52],

$$C_e(T_e)\frac{\partial T_e}{\partial t}=\nabla\cdot(k\nabla T_e)-G(T_e-T_l)+S \tag{22}$$

$$C_l(T_l)\frac{\partial T_l}{\partial t}=G(T_e-T_l) \tag{23}$$

If the characteristic heating time is much longer than the thermalization time, the temperature difference between electrons and the lattice is negligible and the HTS model can be simplified to the hyperbolic one-step model (HOS),

$$C\frac{\partial T}{\partial t}=-\nabla\cdot Q+S \tag{24}$$

$$t\frac{\partial Q}{\partial t}+k\nabla T+Q=0 \tag{25}$$

When the characteristic heating time is much longer than both the electron relaxation time and the electron-lattice thermalization time, the HTS model becomes the conventional Fourier heat conduction model,

$$C\frac{\partial T}{\partial t}=\nabla\cdot(k\nabla T)+S \tag{26}$$

Figure 8 shows a regime map of energy transport mechanisms during laser heating of gold with different heating times and at different temperatures. The onset of nonequilibrium heating and hyperbolic energy transport is chosen as $t_h=5t_c$ and $t_h=5\tau$, respectively. The thermalization time is taken from measurements [53]. The relaxation time is estimated from the formula [23]

$$k(T)=\frac{\pi^2 n\kappa^2\tau(T)}{3m_e}T \tag{27}$$

by using the compiled thermal conductivity data [54] and reported physical constants [23]. The HTS model provides a general, united picture about energy transport during laser heating. The POS model applies for slow heating processes, the PTS model applies for fast heating processes at high-temperatures, and the HOS model applies for fast heating processes at low-temperatures. In certain low-temperature fast heating regimes, none of the previous models are applicable, and the current HTS model must be used. Figure 9 shows the comparison of predicted electron temperature changes ($\Delta T_e$) with experimental data at the front surface of gold films during 100 femtosecond laser pulse heating. The HTS model agrees well with experimental results. Further studies on radiation deposition and transport mechanisms in semiconductors, dielectrics, and bio-materials are necessary.

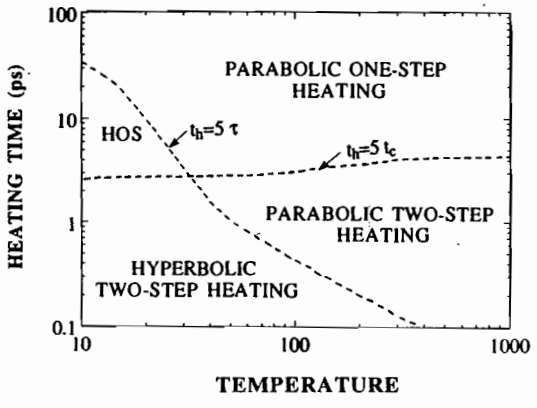


**Figure 8** Regime map for laser heating of gold

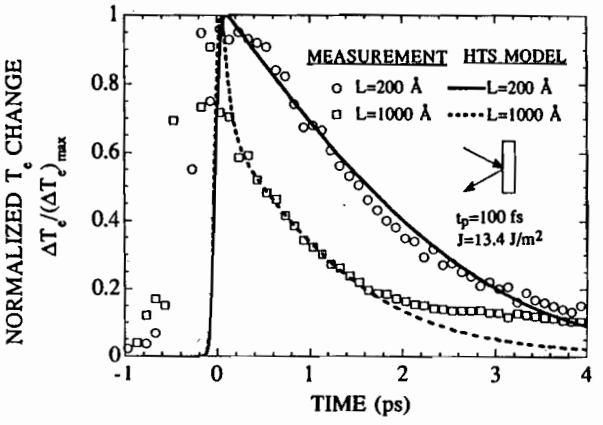


**Figure 9** Electron-temperature changes during 100 fs laser pulse heating

## 4.2 Novel Applications

The invention of optical microscopes increased the spatial resolution of optical observations from sub-millimeters to micrometers, having a great impact on the development of technology and medicine. Like microscopes, the rapid development of high-power and short-pulse lasers has also brought human beings from a macroscale world into a microscale world, increasing the temporal resolution of the observation of phenomena and manipulation of processes. Temporal resolution has increased from microseconds to femtoseconds, approaching the time limit of molecular-level processes.As a result, high-power and short-pulse lasers have generated new techniques in many areas, including high-speed thermal diagnostics, short-pulse laser processing, and short-pulse imaging

Short-pulse lasers provide high-speed thermal diagnostic techniques. Examples include high-speed thermometry [5, 55], observation and measurement of fast melting [56, 57], femtosecond imaging of melting and evaporation [58], and direct measurements of energy distributions at the molecular scale [59]. Two different operation modes of high-speed thermal diagnostics exist. One is the *transient measurement mode* which detects the whole transient history of a thermal process. The other is the *fixed-delay-time measurement mode* which only measures the variation after a certain time delay. The transient mode has the advantage of providing real time measurements; however, it has relatively low temporal resolution. Its overall temporal resolution is limited to about one nanosecond as set by the response time of each individual signal detection, conversion and recording device. On the other hand, the fixed-delay-time mode can achieve a much higher temporal resolution, reaching femtoseconds using short laser pulses as thermal probes. An intense light pulse (pump pulse) is used to heat the material, and then a second pulse (probe pulse) with a preset time delay is used to detect the signal. By repeating the measurement with different delay times in an identical heating processes, a statistical picture of the transient thermal process can be reconstructed. Temporal resolution relies on the duration of the laser pulses and accurate control of the time delay. Table 1 summarizes the major features of these two different operation modes. High-speed thermal diagnostic techniques are expected to play a significant role in gaining fundamental information about thermal phenomena.

**Table 1** High-speed thermal diagnostics techniques

| | Transient Mode | Fixed Delay-Time Mode |
|---|---|---|
| Features | Entire measurement of a single event | Statistical average of numerous events |
| Limiting factors | Speed of detectors and data acquisition | Pulse duration |
| Achievable resolution | ~1 ns | ~30 fs |
| Key devices | High-speed detectors and data acquisition systems | Short-pulse lasers |

Applications of high-power and short-pulse lasers have generated new material processing techniques based on their unique features. The short laser pulse duration and the small laser beam diameter make them suitable for microfabrication in many areas [60, 61]. Examples include laser micro-drilling [62, 63], laser repair of microelectronic circuits [50], laser planarization in fabrication of very-large-scale-integration chips (VLSI) [4], and laser removal of contamination particles from surfaces [64, 65]. The high heating and cooling rates in laser hardening and laser cladding processes produce novel materials that often possess a high degree of hardness and are highly resistant to corrosion and wear. The high laser intensity also makes it possible to process transparent materials through nonlinear radiation absorption processes [66]. The extreme nonequilibrium conditions created by pulsed-laser evaporation of target materials allow *in-situ* preparation of a wide variety of high-quality thin films [67]. One particular area in which the pulsed-laser technique has advantages over other thin film deposition techniques is the preparation of high-temperature superconducting (HTS) thin films, where it preserves the stoichiometry of the multicomponent HTS materials during fabrication [68]. Successful operation of these techniques requires a thorough understanding and active control of thermal phenomena in the micro-time scale.

Short-pulse lasers also provide novel imaging techniques for scattering media, such as biological tissues. The propagation of light has finite speed; it takes one picosecond for light to travel 300 μm in vacuum. By measuring the arrival time of a light pulse, the path length of the light pulse can be calculated; and by further considering the time history of the arrival pulse, the path of the light pulse can be constructed, providing an imaging technique [69, 70]. The image reconstruction process is a reverse radiation transfer problem, requiring a better understanding of the interactions of short laser pulses with small structures and propagation of these pulses in scattering media. It presents new challenges and opportunities for thermal engineers.

## Acknowledgments

The authors acknowledge the financial support from the U.S. National Science Foundation, the U.S. Department of Energy, and the K.C. Wang Education Foundation in Hong Kong.

## Reference

[1] Goodson, K.E., and Flik, M.I., "Effect of Microscale Thermal Conduction on the Packing Limit of Silicon-on-Insulator Electronic Devices," *IEEE Transactions on Components Hybrids and Manufacturing Technology*, **15** (1992), 715-722.

[2] Tsubouchi, K., Utsugi, S., Futatsuya, T., and Mikoshiba, N., "Theoretical Analysis for a New Package Concept — High-Speed Heat Removal For VLSI Using an AlN Heat-Spreading Layer and Microchannel Fin," *Japanese Journal of Applied Physics Part 2*, **30** (1991), L88-L91.

[3] Fricke, J., Lu, X., Wang, P., Buttner, D., and Heinemann, U., "Optimization of Monolithic Silica Aerogel Insulants," *International Journal of Heat and Mass Transfer*, **35** (1992), 2305-2309.

[4] Carey, P.G., Woratschek, B.J., and Bachmann, F., "Progress Toward Excimer Laser Metal Planarization and Via Hole Filling Using In-Situ Monitoring," *Microelectronic Engineering*, **20**

(1993), 89-106.
[5] Eesley, G.L., "Picosecond Dynamics of Thermal and Acoustic Transport in Metal Films," *International Journal of Thermophysics,* 11 (1990), 811-817.
[6] Chen, G., and Tien, C.L., "Thermal Conductivity of Quantum Well Structures," *Journal of Thermophysics and Heat Transfer,* 7 (1993), 311-318.
[7] Majumdar, A., "Microscale Heat Conduction in Dielectric Thin Films," *Journal of Heat Transfer,* 115 (1991), 7-16.
[8] Hesketh, P.J., Zemel, J.N., and Gebhart, B., "Organ Pipe Radiation Modes of Periodic Micromachined Silicon Surfaces," *Nature,* 324 (1986), 549-551.
[9] Hager, J.M., Simmons, S., Smith, D., Onishi, S., Langley, L.W., and Diller, T.E., "Experimental Performance of a Heat Flux Microsensor," *Journal of Engineering for Gas Turbines and Power,* 113 (1991), 246-250.
[10] Fricke, J., "Thermal Transport in Porous Superinsulations," *Aerogels,* J. Fricke, ed., Springer Verlag, Berlin, (1986), 94-103.
[11] Akhmanov, S.A., Vysloukh, V.A., and Chirkin, A.S., *Optics of Femtosecond Laser Pulses,* American Institute of Physics, New York, (1992).
[12] Herrmann, J., and Wilhelmi, B., *Lasers for Ultrashort Light Pulses,* North-Holland, Amsterdam, (1987).
[13] Fork, R.L., Brito, J.Y., Cruz, C.H., Becker, P.C., and Shank, C.V., "Compression of Optical Pulses to Six Femtoseconds by Using Cubic Phase Compensation," *Optics Letters,* 12 (1987), 483-485.
[14] Cho, D., Warrington, D., Jr., Pisano, A., Bau, H., Friedrich, C., Jara-Almonte, J., and Liburdy, J., eds., *Micromechanical Sensors, Actuators, and Systems,* ASME SDC 32 (1991).
[15] Udell, K., Buckius, R.O., and Gerner, F., eds., *Heat Transfer on the Microscale,* ASME HTD 200 (1992).
[16] Born, M., and Wolf, E., *Principles of Optics,* 6th Edition, Pergamon Press, Oxford, (1980).
[17] Grubin, H.L., Ferry, D.K., and Jacoboni, C., eds., *The Physics of Submicron Semiconductor Devices,* Plenum Press, New York, (1983), 521-576.
[18] Yariv, A., *Quantum Electronics,* John Wiley & Sons, New York, (1989).
[19] Tien, C.L., and Chen, G., "Challenges in Microscale Radiative and Conductive Heat Transfer," to appear in *Journal of Heat Transfer* (1993).
[20] Tien, C.L., and Lienhard, J.H., *Statistical Thermodynamics,* Hemisphere, Washington D.C., (1979).
[21] Gurevich, V.L., *Transport in Phonon Systems,* Elsevier, New York, (1986), 110-152.
[22] Flik, M.I., Choi, B.I., and Goodson, K.E., "Heat Transfer Regimes in Microstructures," *Journal of Heat Transfer,* 114 (1992), 666-674.
[23] Kittel, C., *Introduction to Solid State Physics,* 6th edition, John Wiley & Sons, Inc., New York, (1986).
[24] Qiu, T.Q., and Tien, C.L., "Heat Transfer Mechanisms during Short-Pulse Laser Heating of Metals," to appear in *Journal of Heat Transfer* (1993).
[25] Dharssi, I., Butcher, P.N., and Warren, G., "Mobility and Hall Factor Calculations for a Superlattice," *Superlattices and Microstructures,* 9 (1991), 335-339.
[26] Wakuri, S., and Kotake, S., "Molecular Dynamics Study of Heat Transfer in Very Thin Films," *ASME/JSME Thermal Engineering Proceedings,* 4 (1991), 111-116.
[27] Metha, C.L., "Coherence-Time and Effective Bandwidth of Blackbody Radiation," *Nuovo Cimento,* 21 (1963), 401-408.
[28] Tien, C.L., "Thermal Radiation in Packed and Fluidized Bed," ASME *Journal of Heat Transfer,* 110 (1988), 1230-1242.
[29] Tuntomo, A., Tien, C.L., and Park, S.H., "Internal Distribution of Radiation Absorption in a Spherical Particle," *Journal of Heat Transfer,* 113 (1991), 407-412.
[30] Chen, G., and Tien, C.L., "Partial Coherence Theory of Thin Film Radiative Properties," *Journal of Heat Transfer,* 114 (1992), 636-643.
[31] Richter, K., Chen, G., and Tien, C.L., "Partial Coherence Theory of Multilayer Thin-Film Optical Properties," to appear in *Optical Engineering* (1993).
[32] Siegel, R., and Howell, J.R., *Thermal Radiation Heat Transfer,* 3rd Edition, Hemisphere, Washington D.C., (1992).
[33] Monreal, R., Garcia-Moliner, F., and Flores, F., "Non Local Electrodynamics of Metal Film Systems," *Journal de Physique,* 43 (1982), 901-913.
[34] Ziman, J.M., *Electrons and Phonons,* Clarendon Press, Oxford, (1960).
[35] Brinker, C.J., and Scherer, G.W., *Sol-Gel Science,* Academic Press, San Diego, (1990).
[36] Fricke, J., "Aerogels - A Fascinating Class of High-Performance Porous Solids," *Aerogels,* J. Fricke, ed., Springer-Verlag, Berlin, (1986), 2-19.
[37] Kistler, S.S., "Coherent Expanded Aerogels and Jellies," *Nature,* 127 (1931), 741.
[38] Meakin, P., "Models for Colloidal Aggregation," *Annual Review of Physical Chemistry,* 39 (1988), 237-266.
[39] Schaefer, D.W., and Keefer, K.D., "Structure of Soluble Silicates," *Better Ceramics through Chemistry,* C.J. Brinker, D.E. Clark, and D.R. Ulrich, eds., North Holland, (1984), 1-14.
[40] Scheuerpflug, P., Morper, H., Neubert, G., and Fricke, J., "Low Temperature Thermal Transport in Silica Aerogels," Journal of Physics D: Applied Physics, 24 (1991), 1395-1403.
[41] Kistler, S.S., "The Calculation of the Surface Area of Microporous Solids from Measurements of Heat Conductivity," *Journal of Physical Chemistry,* 46 (1942), 19-31.
[42] Rubin, M., and Lampert, C.M., "Transparent Silica Aerogels for Window Insulation," *Solar Energy Material,* 7 (1983), 393-400.
[43] Schmitt, W.J., "The Preparation and Properties of Acid Catalyzed Silica Aerogels," M.Sc. Thesis, Department of Chemanical Engineering, University of Wisconsin, Madison, (1981).
[44] Boy, E., Munding, M., and Wittwer, V., "Experimental Investigations on the Performance of Granular $SiO_2$ Aerogels as a Transparent Insulation of Mass Walls," *Journal de Physique,* 50 (1989), C499-C4105.
[45] Goetzberger, A., and Wittwer, V., "Translucent Insulation for Passive Solar Energy Utilization in Buildings," *Aerogels,* J. Fricke, ed., Springer Verlag, Berlin, (1986), 84-93.
[46] Schreiber, E., Boy, E., and Bertsch, K., "Aerogel as a Transparent Thermal Insulation Material for Buildings," *Aerogels,* J. Fricke, ed., Springer Verlag, Berlin, (1986), 133-139.
[47] Pajonk, G.M., "Aerogel Catalysts," *Applied Catalysis,* 72 (1991), 217-266.
[48] Fournier, D., and Boccara, A.C., "Heat Diffusion and Random Media," *Topics in Current Physics,* Springer-Verlag, Berlin, (1989), 303-312.
[49] Letokhov, V.S., and Ustinov, N.D., *Power Lasers and Their Applications,* Harwood Academic Publishers, New York, (1983).
[50] Kolinsky, P.V., Fluxman, S.M., King, R.A., and Wood, R.M., "Laser Repair of Active Matrix Display Drive Circuits," *Electronics Letters,* 28 (1992), 2202-2204.
[51] Chlipala, J.D., Scarfone, L.M., and Lu, C., "Computer-Simulated Explosion of Poly-Silicide Links in Laser-Programmable Redundance for VLSI Memory Repair," *IEEE Transactions on Electron Devices,* 36 (1989), 2433-2439.
[52] Anisimov, S.I., Kapeliovich, B.L., and Perel'man, T.L., "Electron Emission from Metal Surfaces Exposed to Ultrashort Laser Plulses," *Soviet Physics JETP,* 39 (1974), 375-377.
[53] Groeneveld, R.H.M., "Femtosecond Spectroscopy on Electrons and Phonons in Noble Metals," Ph.D thesis, Van der Waals - Zeeman Laboratory, University of Amsterdam, (1992).
[54] Powell, R.W., and Ho, C.Y., "The State of Knowledge Regarding the Thermal Conductivity of the Metallic Elements," *Thermal Conductivity,* D.R. Flynn et al. eds., National Bureau of Standards, Gaithersburg, Maryland, (1969), 1-31.
[55] Elsayed-Ali, H.E., and Herman, J.W., "Picosecond Time-Resolved Surface-Lattice Temperature Probe," *Applied Physics Letters,* 57 (1990), 1508-1510.
[56] Schroder, T., Rudolph, W., Goborkov, S.V., and Shumay, I.L., "Femtosecond Laser-Induced Melting of GaAs Probed by Optical Second-Harmonic Generation," *Applied Physics A,* 51 (1990), 49-51.
[57] Herman, J.W., and Elsayed-Ali, H.E., "Superheating of Pb (111)," *Physical Review Letters,* 69 (1992), 1228-1231.
[58] Downer, M.C., Fork, R.L., and Shank, C.V., "Femtosecond Imaging of Melting and Evaporation at a Photoexcited Silicon Surface," *Journal of Optical Society of America Part B,* 2 (1985), 595-599.
[59] Fann, W.S., Storz, R., Tom, H.W.K., and Brokor, J., "Direct Measurement of Nonequilibrium Electron-Energy Distributions in Sub-Picosecond Laser-Heated Gold Films," *Surface Science,* 283 (1993), 221-225.
[60] Boyd, I.W., *Laser Processing of Thin Films and Microstructures,* Springer-Verlag, Berlin (1987).

[61] Ehrlich, D.J., and Tsao, J.Y., ed., *Laser Microfabrication*, Academic, Boston, (1989).

[62] Kestenbaum, A., Damico, J.F., Blumenstock, B.J., and Deangelo, M.A., "Laser Drilling of Microvias in Epoxy-Glass Printed Circuit Boards," *IEEE Transactions on Components Hybrids and Manufacturing Technology*, 13 (1990), 1055-1062.

[63] Riley, S., and Schick, L., "Laser Drilling Vias in GaAs Wafers," *Lasers in Microelectronic Manufacturing*, SPIE 1598, (1991), 118-120.

[64] Lee, S.J., Iman, K., and Allen, S.D., "Laser-Assisted Particle Removal from Silicon Surfaces," *Microelectronic Engineering*, **20** (1993), 145-157.

[65] Zapka, W., Ziemlich, W., Leung, W.P., and Tam, A.C., "'Laser Cleaning' Removes Particles from Surfaces," *Microelectronic Engineering*, 20 (1993), 171-183.

[66] Kuper, S., and Stuke, M., "Ablation of UV-Transparent Materials with Femtosecond UV Excimer Laser Pulses," *Microelectronic Engineering*, 9 (1989), 475-480.

[67] Cheung, J.T., and Sankur, H., "Growth of Thin Films by Laser-Induced Evaporation," *CRC Critical Reviews in Solid State and Materials Sciences*, 15 (1988), 63-109.

[68] Habermeier, H.-U., "Y-Ba-Cu-O High Temperature Superconductor Thin Film Preparation by Pulsed-Laser Deposition: Recent Developments," *Materials Science and Engineering Part B*, 13 (1992), 1-7.

[69] Yoo, K.M., Das, B.B., and Alfano, R.R., "Imaging of Translucent Object Hidden in a Highly Scattering Medium from the Early Portion of the Diffuse Component of a Transmitted Ultrafast Laser Pulse," *Optics Letters*, 17 (1992), 958-960.

[70] Feng, L., Yoo, K.M., and Alfano, R.R., "Ultrafast Laser-Pulse Transmission and Imaging through Biological Tissues," *Applied Optics*, 32 (1993), 554-558.